



1 Seasonal prediction skill of East Asian summer monsoon in CMIP5-Models

2 **Bo Huang,\* Ulrich Cubasch, Christopher Kadow**

3 **Institute of Meteorology, Freie Universität Berlin,**  
4 **Carl-Heinrich-Becker-Weg 6-10, 12165 Berlin, Germany**

5 **Email: [huangb@zedat.fu-berlin.de](mailto:huangb@zedat.fu-berlin.de)**

6

7 **ABSTRACT**

8 The East Asian summer monsoon (EASM) is an important part of the global climate system  
9 and plays a vital role in the Asian climate. Its sub-seasonal-to-seasonal predictability is a  
10 long-standing issue within the monsoon scientist community. In this study, we analyse the  
11 seasonal (with six months lead time) prediction skill of the EASM rainfall and its associated  
12 general circulation in non-initialised and initialised simulations for the years 1979-2005  
13 performed by six prediction systems (*i.e.*, the BCC-CSM1-1, the CanCM4, the GFDL-  
14 CM2p1, the HadCM3, the MIROC5 and the MPI-ESM-LR) from the Coupled Model  
15 Intercomparison Project phase 5 (CMIP 5). We find that the simulation of the zonal wind is  
16 significantly improved in initialised simulations compared to non-initialized simulations.  
17 Based on the knowledge that zonal wind indices can be used as potential predictors for the  
18 EASM, we selected an EASM index based upon the zonal wind for further analysis. The  
19 assessment show that the GFDL-CM2p1 and the MIROC5 add prediction skill in simulating  
20 the EASM index with initialisation, the BCC-CSM1-1, the CanCM4, and the MPI-ESM-LR  
21 change the skill insignificantly, and the HadCM3 indicates a decreased skill score. The  
22 different response to the initialisation can be traced back to the ability of the models to  
23 capture the ENSO (El Niño-Southern Oscillation)-EASM coupled mode, particularly the  
24 Southern Oscillation-EASM coupled mode. In summary, we find that the GFDL-CM2p1 and  
25 the MIROC5 are capable to predict the EASM on a seasonal time-scale after initialisation.

26 **Key Words:** East Asian summer monsoon; initialisation; seasonal prediction; ENSO-EASM  
27 coupled mode; CMIP5



28 **1. INTRODUCTION**

29 The Asian monsoon is the most powerful monsoon system in the world due to the thermal  
30 contrast between the Eurasian continent and the Indo-Pacific Ocean. Its evolution and  
31 variability critically influences the livelihood and the socio-economic status of over two  
32 billion residents who live in the Asian monsoon dominated region. It encompasses two sub-  
33 monsoon systems (e.g., South Asian monsoon-SAM and East Asian monsoon-EAM; Wang,  
34 2006). In summer time (June-July-August), the EAM, namely, the East Asian summer  
35 monsoon (EASM) occurs from the Indo-China peninsula to the Korean Peninsula and Japan,  
36 and shows strong intraseasonal-to-interdecadal variability (Ding and Chan, 2005). Thus,  
37 accurate predictions of the EASM is an important and long-standing issue in climate science.

38 To predict the EASM, there are two approaches, statistical prediction and dynamical  
39 prediction, respectively. The statistical method seeks the relationship between the EASM and  
40 a strong climate signal (e.g., ENSO, NAO; Wang et al., 2015;Wu et al., 2009;Yim et al.,  
41 2014). This method is limited by the strength of the climate signal. The other method is  
42 dynamical prediction. It employs climate model to predict the EASM (Kang and Yoo,  
43 2006;Lee et al., 2010;Sperber et al., 2001;Wang et al., 2008a;Yang et al., 2008;Kim et al.,  
44 2012). Two kinds of climate models have been developed in the past few decades,  
45 atmosphere general circulation model (AGCM) and coupled atmosphere-ocean general  
46 circulation model (AOGCM). Both the two kinds of model have been used to predict the  
47 EASM (Kang et al., 2004;Wang et al., 2005;Wang et al., 2007;Wang et al., 2008a;Zhou et al.,  
48 2009). For AGCMs, the lower boundary conditions (*e.g.* SST: sea surface temperature) is  
49 required. An external ocean model is applied to predict the SST. Then the prescribed SST is  
50 employed as the lower boundary conditions to force the AGCMs. However, this method  
51 shows a low prediction skill over East Asia, especially in monsoon season (Wang et al.,  
52 2005;Barnston et al., 2010), because the AGCMs fail to produce the realistic SST-rainfall  
53 relationships in monsoon season (Wang et al., 2005;Wang et al., 2004). Therefore, the  
54 monsoon community endeavours to predict the EASM with AOGCMs (Zhou et al.,  
55 2009;Wang et al., 2008a;Jiang et al., 2013;Kim et al., 2012).

56 AOGCMs have proved to be the most valuable tools in predicting the EASM (Zhou et  
57 al., 2009;Wang et al., 2008a;Jiang et al., 2013;Kim et al., 2012). However, the performance  
58 of AOGCMs in predicting the EASM on seasonal time-scale strongly depends on their ability  
59 to reproduce the teleconnection between EASM and SST (Sperber et al., 2001) and the  
60 initialisation (Wang et al., 2005). In the coupled model inter-comparison project (CMIP)



61 phase 3 (CMIP3; Meehl et al., 2007) era, the models simulate not only a too weak SST-  
62 monsoon teleconnection (Kim et al., 2008; Kim et al., 2011), but also a too weak East Asian  
63 zonal wind-rainfall teleconnection (Sperber et al., 2013). Compared to CMIP3 models, CMIP  
64 phase 5 (CMIP5; Taylor et al., 2012) models improve the representation of monsoon status  
65 (Sperber et al., 2013). Therefore, given initial conditions, the CMIP5 models have potential to  
66 predict the EASM.

67 Initial conditions play a vital factor in predicting the EASM on sub-seasonal to  
68 seasonal time-scale (Kang and Shukla, 2006). Under current set up of initialisation, the  
69 CMIP5 models show the ability to predict the SST indicator (*i.e.*, El Niño-Southern  
70 Oscillation-ENSO index) up to 15 months in advance (Choi et al., 2016; Meehl et al.,  
71 2014; Meehl and Teng, 2012). This extended prediction skill of the ENSO suggests that the  
72 EASM can be predicted on a seasonal time-scale if the dynamic link between the ENSO and  
73 monsoon circulations is well represented in these models. Two scientific questions will be  
74 addressed in this study: 1. How realistic are the initialized CMIP5 models in representing the  
75 EASM? 2. To what extent reproduce the model's teleconnection between the ENSO and the  
76 EASM?

77 In this paper, we inter-compare the influence of the initialisation on the capability of  
78 the CMIP5 model to capture the EASM and the ENSO-EASM teleconnections. The model  
79 simulations, comparison data and methods are introduced in Section 2. Section 3 describes  
80 the seasonal skill of the rainfall predictions and the prediction of the associated general  
81 circulation of the EASM. The mechanism causing the differential response of the models to  
82 the initialisation is presented in Section 4. The main conclusions and discussions are  
83 summarised in Section 5.

## 84 **2. MODELS, DATA AND METHODS**

### 85 **2.1 MODELS AND INITIALISATION**

86 In this study, we assess six prediction systems which have contributed to CMIP5 in historical  
87 and decadal hindcast simulations (Table 1). We employ these six prediction systems of  
88 CMIP5 in our study which have performed a yearly initialisation. Only these systems provide  
89 data to study the effect of initialisation on seasonal time-scale. The BCC-CSM1-1 has three  
90 ensemble members which are initialised on 1st September, 1st November and 1st January,  
91 respectively. The initialisation of HadCM3 takes place on each pre-year 1st November while  
92 the other four systems are initialised on 1st January. The full-field initialisation is named  
93 HadCM3-ff to distinguish it from the anomaly initialisation in HadCM3. Because of spatial



94 coverage of the precipitation observations, we select the satellite era (1979 to 2005) for our  
95 study. The first lead year results from initialised simulations are used to assess the seasonal  
96 predicting skills of the CMIP5 models. The initialisation strategies of all modelling groups  
97 from CMIP5 decadal prediction experiments have been summarised in Meehl *et al.* (2014).  
98 The brief configurations of the six prediction systems are presented in Table 2.

## 99 2.2 COMPARISON DATA

100 The main datasets which are used for the comparison in this study include: (1)  
101 monthly precipitation data from the Global Precipitation Climatology Project (GPCP; Adler  
102 et al., 2003); (2) monthly circulation data from ECMWF Interim re-analysis (ERA-Interim;  
103 Dee et al., 2011); and (3) monthly mean SST from National Oceanic and Atmospheric  
104 Administration (NOAA) improved Extended Reconstructed SST version 4 (ERSST v4;  
105 Huang et al., 2015). All the model data and the comparison data are remapped onto a  
106 common grid of 2.5°x2.5° by bi-linear interpolation to reduce the uncertainty induced by  
107 different data resolutions.

## 108 2.3 METHODS

109 We apply the pattern correlation coefficient (PCC) to analyse the model performance  
110 in capturing the spatial pattern with reference to the observational data. It is the Pearson  
111 product-moment coefficient of linear correlation between a single variables on two different  
112 spatial patterns (Barnett and Schlesinger, 1987). There are two types of pattern correlation  
113 statistics: centred and un-centred. The centred (un-centred) statistic measures the similarity of  
114 two patterns after (without) the removal of the global mean. We choose the un-centred PCC  
115 in our study due to the fact that centred correlations alone are not sufficient for the attribution  
116 of seasonal prediction (Mitchell et al., 2001). The un-centred PCC is defined by:

$$PCC = \frac{\sum_{x=1}^n \sum_{y=1}^m w_{(x,y)} F_{(x,y)} A_{(x,y)}}{\sqrt{\sum_{x=1}^n \sum_{y=1}^m w_{(x,y)} F_{(x,y)}^2 \sum_{x=1}^n \sum_{y=1}^m w_{(x,y)} A_{(x,y)}^2}}$$

117

118 where n and m are grids on longitude and latitude, respectively.  $F_{(x,y)}$  and  $A_{(x,y)}$  represent two  
119 dimensions comparison and validating value.  $w_{(x,y)}$  indicates the weighting coefficient for  
120 each grid. An equal weighting coefficient was applied due to the study area is East Asia  
121 where we can omit the convergence of the longitudes with the latitudes

122 We also employ the anomaly correlation coefficient (ACC) to analyse the model  
123 performance in reproducing observational variations. The ACC is the correlation between



124 anomalies of forecasts and those of verifying values with the reference values, such as  
 125 climatological values (Drosowsky and Zhang, 2003). Its definition is:

$$ACC = \frac{\sum_{i=1}^n w_i (f_i - \bar{f})(a_i - \bar{a})}{\sqrt{\sum_{i=1}^n w_i (f_i - \bar{f})^2 \sum_{i=1}^n w_i (a_i - \bar{a})^2}}, (-1 \leq ACC \leq 1)$$

126

$$f_i = F_i - C_i, \bar{f} = \left( \sum_{i=1}^n w_i f_i \right) / \sum_{i=1}^n w_i$$

127

$$a_i = A_i - C_i, \bar{a} = \left( \sum_{i=1}^n w_i a_i \right) / \sum_{i=1}^n w_i$$

128

129 where  $n$  is the number of number of samples, and  $F_i$ ,  $A_i$ ,  $C_i$  represent comparison, verifying  
 130 value, and reference value such as climatological value, respectively. Also,  $\bar{f}$  is the mean of  
 131  $f_i$ ,  $\bar{a}$  is the mean of  $a_i$ , and  $w_i$  indicates the weighting coefficient. If the variation of anomalies  
 132 of comparison dataset is perfectly coincident with that of the anomalies of verifying value,  
 133 ACC will take 1 (the maximum value). Otherwise, if the variation is completely reversed,  
 134 ACC is -1 (the minimum value).

135 The root-mean-square-error (RMSE) is employed to check the model deviation from  
 136 the observation and its definition is:

$$RMSE = \sqrt{\sum_{i=1}^n w_i D_i^2} / \sqrt{\sum_{i=1}^n w_i}$$

137

138 where  $D_i$  represents the deviation between comparison and verifying value,  $w_i$  is the  
 139 weighting coefficient for each sample, and  $n$  is the number of samples. If RMSE is closer to  
 140 zero, it means that the comparisons are closer to the verifying values.

### 141 3. SEASONAL PREDICTION SKILL OF THE EASM

142 The EASM has complex spatial and temporal structures that encompass the tropics,  
 143 subtropics, and midlatitudes (Tao and Chen, 1987; Ding, 1994). In late spring, an enhanced  
 144 rainfall pattern is observed in the Indochina Peninsula and in South China Sea. Then, the  
 145 rainfall belt advances northwards to the south of China. In early summer, the rainfall  
 146 concentration occurs in the Yangtze River Basin and in southern Japan, namely, the Meiyu



147 and Baiu season, respectively. The rainfall belt can reach as far as northern China, the Korean  
148 Peninsula (called the Changma rainy season) and central Japan in July (Ding, 2004;Ding and  
149 Chan, 2005).

150 The EASM is characterised by both seasonal heterogeneous rainfall distribution and  
151 associated large-scale circulation systems (Wang et al., 2008b). In the summer season, water  
152 moisture migrates from the Pacific Ocean to central and eastern Asia, which is carried by the  
153 southwest surface winds. Generally, a strong summer monsoon year is followed by  
154 precipitation in northern China, while a weak summer monsoon year is usually accompanied  
155 by heavier rainfall along the Yangtze River basin (Zhou and Yu, 2005;Ding, 1994).

156 The prediction skill of the EASM rainfall and the associated general circulation  
157 variable (*i.e.*, zonal and meridional wind, and mean sea level pressure) is presented in Figure  
158 1. These variables are resource of monsoon index (Wang et al., 2008b). Table 3 shows the  
159 contribution of these variables in the EASM. Their abbreviations follow the guideline of  
160 CMIP5 (Taylor et al., 2012). Without initialisation, the models show an acceptable  
161 performance in capturing the observed spatial variation (with high PCC) of the six variables,  
162 but a poor performance in simulating their temporal variation (with low ACC). After  
163 initialisation, we can see that the models show a higher ACC of the six variables. However,  
164 there is no improvement in simulating the spatial variation (PCC). The improvement of  
165 simulating the temporal variation of zonal winds (*i.e.*, ua850 and ua200) is larger than of the  
166 rainfall and meridional winds. One can exploit this improvement by using, a general  
167 circulation based monsoon index as a tool to predict the EASM.

168 In the recent decades, more than 25 general circulation indices have been produced to  
169 research the variability and long-term change of the EASM. Wang *et al.* (2008) classified  
170 them into five categories and discussed their ability to capture the main features of the  
171 EASM. They found that the Wang and Fan index (hereafter WF-index; 1999) shows the best  
172 performance in capturing the total variance of the precipitation and three-dimensional  
173 circulation over East Asia. We, thus, select the WF-index for the further analysis. Its  
174 definition is standardised average zonal wind at 850 hPa in (5°-15°N, 90°-130°E) minus in  
175 (22.5°-32.5°N, 110°-140°E). The WF-index is a shear vorticity index which often described  
176 by a north-south gradient of the zonal winds. In positive (negative) phase of the WF-index  
177 years, two strong (weak) rainfall belts locate at the Indo China Peninsula-to-the Philippine  
178 Sea and the northern China-to-the Japan Sea, and a weak (strong) rainfall belt occurs from the  
179 Yangtze river basin-to-the south of Japan.



180 In the non-initialised simulations, none of the models captures the observed EASM, as  
181 indicated by an insignificant ACC (Figure 2). The CanCM4 and the GFDL-CM2p1 simulate  
182 a negative phase, while the BCC-CSM1-1, the HadCM3, the MIROC5 and the MPI-ESM-LR  
183 all predict a positive phase of the EASM. After initialisation, the CanCM4, the GFDL-  
184 CM2p1 and the MIROC5 improve the skill to simulate the EASM, the MPI-ESM-LR  
185 displays hardly any reaction, while the BCC-CSM1-1 and the HadCM3 shows a worse  
186 performance than before. Particularly with anomaly initialisation, the HadCM3 significantly  
187 loses its prediction skill in capturing the EASM.

#### 188 4. EASM-ENSO COUPLED MODE IN CMIP5

189 We employ the EOF method to analyse the leading EOF modes of six meteorological  
190 variables anomaly in the EASM region ( $0^{\circ}$ - $50^{\circ}$ N,  $100^{\circ}$ - $140^{\circ}$ E). The first EOF mode of  
191 rainfall is characterised by a “sandwich” pattern which shows sharp contrast between the  
192 prominent rainfall centre over Malaysia, the Yangtze River valley and the south of Japan, and  
193 the enhanced rainfall over the Indo-China Peninsula and the Philippine Sea. The increased  
194 precipitation is associated with cyclones in the low-level (850 hPa) and anti-cyclones in the  
195 upper level (200 hPa) (not shown).

196 The correlation coefficient of the first eigenvector and the associated principal  
197 component (PC) between the model simulation and the observation in the non-initialised and  
198 the initialised simulation is presented in Figure 3. The models can capture the eigenvector of  
199 the first EOF for the six meteorological fields in non-initialised simulation. However, they  
200 fail to reproduce the associated PC of the first leading EOF mode. Compared to the non-  
201 initialised simulation, the models show no improvement to simulate the first leading EOF  
202 mode of rainfall, but exhibit a better performance in representing the first leading EOF mode  
203 of zonal wind. The CanCM4 and the GFDL-CM2p1 capture the first PC of ua850, but not the  
204 other five models. For the zonal wind at 200 hPa, the BCC-CSM1-1 fails to simulate its first  
205 EOF mode while the other six models can. Then, only the GFDL-CM2p1 accurately  
206 simulates the first EOF eigenvectors and the associated PC of va850, which cannot be  
207 reproduced in the other models. None of the models captures the spatial-temporal variation of  
208 the first EOF mode of meridional wind at 200 hPa. In addition, the GFDL-CM2p1 and the  
209 MIROC5 simulates a reasonable leading EOF mode and associated PC of psl, while the other  
210 models do not capture it.

211 Figure 4 shows the fractional (percentage) variances of the six variables of the first  
212 EOF mode with the total variances from the observation, and the model simulation in non-



213 initialisation and in initialisation. The observational total variances for the pr, the ua850, the  
214 ua200, the va850, the va200 and the psl, are depicted by the first lead EOF mode in 21.2,  
215 59.0, 36.5, 20.6, 28.5 and 50.0 percent, respectively. The models simulate the comparable  
216 explanatory variances, which show a slight discrepancy for the first leading mode in the non-  
217 initialisation. From non-initialised simulation to initialised simulation, the CGCMs tend to  
218 enhance the first EOF lead mode due to the fact that they show larger fractional variances of  
219 the total variances of the six variables. We note that the CanCM4 and the GFDL-CM2p1  
220 significantly increase the fractional variances from non-initialisation to initialisation.

221         The ENSO is a dominant mode of the inter-annual variability of the coupled ocean  
222 and atmosphere climate system, which has strong effects on the inter-annual variation of the  
223 EASM (Wu et al., 2003; Wang et al., 2000). Wang et al. (2015) summarised the first EOF  
224 lead mode of the ASM is the ENSO developing mode. As previously mentioned, the first  
225 EOF mode is improved in the initialised simulations, compared to the non-initialised  
226 simulation. This also can be found in the ENSO indices (Figure 5). Niño3.4 is calculated by  
227 the SST anomaly in the central Pacific (190-240°E, 5°S-5°N), while the southern oscillation  
228 index (SOI) is based upon the anomaly of the sea level pressure differences between Tahiti  
229 (210.75°E, 17.6°S) and Darwin (130.83°E, 12.5°S). To calculate the SOI, we interpolate the  
230 grid data to the Tahiti and the Darwin point by bilinear interpolation.

231         The individual members and their ensemble mean of the six models show a low  
232 correlation coefficient to the observational Niño3.4 and the SOI in the non-initialised  
233 simulations. Niño3.4 and SOI represent the oscillation of two components in the earth  
234 system, the ocean and the atmosphere, respectively. These two indices show strong anti-  
235 phase in the observation, with correlation range is -0.94 to -0.92 for four seasons (DJF,  
236 MAM, JJA, SON; Figure 5). The models describe the anti-correlation between Niño3.4 and  
237 the SOI, but weaker than observed. Compared to the non-initialisation, there is a significant  
238 improvement for models in capturing the observational Niño3.4 and the SOI after  
239 initialisation. Initialisation lowers the spread of ensemble members in predicting Niño3.4 and  
240 the SOI in all the six models. However, initialisation does not prominently change the  
241 correlation between Niño3.4 and the SOI in the model simulations. With initialisation, the  
242 GFDL model shows a weaker correlation between Niño3.4 and the SOI, while the HadCM3  
243 models illustrate a stronger correlation. It is worth mentioning that after initialisation the  
244 ensemble mean of each model outperforms its individual members in capturing Niño3.4 and



245 the SOI. The correlation coefficient between Niño3.4 and the SOI of MME is  $\sim 0.8$  in both  
246 non-initialised and initialised simulations.

247 The EASM strongly relies on the pre-seasons ENSO signal due to the lag response of  
248 the atmosphere to the SST anomaly (Wu et al., 2003). The lead-lag correlation coefficients  
249 between the EASM index and the Niño3.4, and the SOI from JJA(-1) to JJA(+1) are  
250 illustrated in Figure 6. The pre-season Niño3.4 (SOI) presents a significant negative  
251 (positive) correlation to the EASM, while the post-season Niño3.4 (SOI) shows a notable  
252 positive (negative) correlation. This lead-lag correlation coefficient phase is called the  
253 Niño3.4-/SOI-EASM coupled mode (Wang et al., 2008b). In the non-initialised cases, the  
254 models do not produce the teleconnection between the ENSO and the EASM. The CanCM4,  
255 the HadCM3 and the MPI-ESM-LR fail to represent the lead-lag correlation coefficient  
256 difference between pre-/post-season ENSO and EASM. The BCC-CSM1-1, the GFDL-  
257 CM2p1 and the MIROC5 capture the coupled mode of the ENSO and the EASM. However,  
258 the pre-season ENSO has a weak effect on the EASM. Compared to the non-initialised cases,  
259 the MIROC5 and the GFDL-CM2p1 both demonstrate a significant improvement in  
260 simulating Niño3.4 (SOI)-EASM coupled mode in the initialisation. The BCC-CSM1-1, the  
261 HadCM3, and the HadCM3-ff show no improvement, with insignificant correlation between  
262 Niño3.4 (SOI) and the EASM. The CanCM4 and the MPI-ESM-LR indicate a higher  
263 correlation between the EASM and the simultaneous-to-post-season ENSO than to the pre-  
264 season ENSO.

## 265 5. SUMMARY AND DISCUSSION

266 Six earth system models from CMIP5 have been selected in our study. We have analysed the  
267 improvement of the rainfall, the mean sea level pressure, the zonal wind and the meridional  
268 wind in the EASM region from non-initialisation to initialisation. The low prediction skill of  
269 the summer monsoon precipitation is due to the uncertainties of cloud physics and cumulus  
270 parameterisations in the models (Lee et al., 2010; Seo et al., 2015). The models show a better  
271 performance in capturing the inter-annual variability of zonal wind than the precipitation after  
272 initialisation (Figure 1). Thus, the zonal wind index is an additional factor which can indicate  
273 the prediction skill of the model. When, we calculate the WF-index in both non-initialised  
274 and initialised simulations, the GFDL-CM2p1 and the MIROC5 show a significant  
275 advancement in simulating the EASM from non-initialised to initialised simulation with a  
276 lower RMSE and a higher ACC (Figure 2). There is only a slight change in the WF calculated  
277 from the BCC-CSM1-1, the CanCM4 and the MPI-ESM-LR data after initialisation.



278 Compared to the non-initialised simulation, the HadCM3 loses prediction skill, especially  
279 with anomaly initialisation.

280 To test the possible mechanisms of the models' performance in the non-initialisation  
281 and the initialisation, we have calculated the leading mode of the six fields which are  
282 associated to the EASM. The models demonstrate a better agreement with the observational  
283 first EOF mode in the initialised simulations (Figure 3). The first lead mode of zonal wind at  
284 200 hPa shows a significant improvement in the models except the BCC-CSM1-1 with  
285 initialisation. Therefore, a potential predictor might be an index based upon the zonal wind at  
286 200 hPa. Compared to the non-initialisation, the models enhance the first EOF mode with a  
287 higher fraction of variance to the total variance after initialisation (Figure 4). The first EOF  
288 mode of the EASM is the ENSO developing mode (Wang et al., 2015). We have analysed the  
289 seasonal simulating skill of Niño3.4 and the SOI in each model (Figure 5). The models show  
290 a poor performance in representing Niño3.4 and the SOI in the non-initialised simulation.  
291 Initialisation improves the model simulating skill of Niño3.4 and the SOI. The initialised  
292 simulations decrease the spread of ensemble members in the models. We found that there is  
293 no significant change in the models reproducing the correlation between Niño3.4 and the SOI  
294 from non-initialisation to initialisation.

295 In general, the pre-season warm phase of the ENSO (El Niño) leads to a weak EASM  
296 producing more rainfall over the South China Sea and northwest China, and less rainfall over  
297 the Yangtze River Valley and the southern Japan; the cold phase of the ENSO (La Niña)  
298 illustrates a reverse rainfall pattern to El Niño in East Asia. The pre-season Niño3.4 (SOI)  
299 exhibits a strong negative (positive) correlation to the EASM, while the correlation between  
300 the post-season Niño3.4 (SOI) and the EASM illustrates an anti-phase as the pre-season  
301 (Figure 6). In the non-initialised simulations, the models do not capture Niño3.4-/SOI-EASM  
302 coupled mode. We found that only the MIROC5 has the ability to represent the Niño3.4-  
303 EASM coupled mode with initialisation. For the SOI-EASM coupled mode, the GFDL-  
304 CM2p1 and the MIROC5 capture it in the initialisation, while the BCC-CSM1-1, the  
305 HadCM3, the HadCM2-ff, the CanCM4 and the MPI-ESM-LR do not.

306 The model exhibits a better performance in simulating the general circulation of the  
307 EASM with initialisation. Thus, initialisation is helpful in forecasting the EASM on a  
308 seasonal time-scale. There are two initialisation methods in our study, full-field initialisation  
309 and anomaly initialisation (Table 1). The full-field initialisation produces more skilful  
310 predictions on the seasonal time-scale in predicting regional temperature and precipitation



311 (Magnusson et al., 2013;Smith et al., 2013). But, for predicting the EASM, there is no  
312 significant difference between the two methods. We can see that both the GFDL-CM2p1 and  
313 the MIROC5 have a significant improvement in capturing the EASM, with full-field and  
314 anomaly initialisation, respectively. Only the HadCM3 was initialised by the two  
315 initialisation techniques. However, both these two initialised techniques are producing poor  
316 predictions of the EASM with no major differences.

317 The initialisation strategy of the models is to initialise with the observed atmospheric  
318 component (*i.e.*, zonal and meridional wind, geopotential height, *etc.*) and the SST (Meehl et  
319 al., 2009;Meehl et al., 2014;Taylor et al., 2012). With initialisation, the SST conveys its  
320 information via the large heat content of ocean to the coupled system. Therefore, an index  
321 indicating an ocean oscillation like Niño3.4 shows a seasonal-to-decadal prediction skill  
322 (Choi et al., 2016;Luo et al., 2008;Jin et al., 2008). The models studied here demonstrate a  
323 prediction skill in simulating Niño3.4 and the SOI due to this effect. The change of the  
324 correlation between Niño3.4 and the SOI is insignificant from non-initialised to initialised  
325 simulations. We therefore conclude that the relationship between Niño3.4 and the SOI  
326 depends more on the model parameterisation than on the initial condition.

327 Wang *et al.* (2015) found that the second EOF mode of ASM is the Indo-western  
328 Pacific monsoon-ocean coupled mode, the third is the Indian Ocean dipole (IOD) mode, and  
329 the fourth is trend mode. The Indo-western Pacific monsoon-ocean coupled mode is the  
330 atmosphere-ocean interaction mode (Xiang et al., 2013;Wang et al., 2013), which is  
331 supported by positive thermodynamic feedback between the western North Pacific (WNP)  
332 anticyclone and the underlying Indo-Pacific sea surface temperature anomaly dipole over the  
333 warm pool (Wang et al., 2015). The IOD increases the precipitation from the South Asian  
334 subcontinent to south-eastern China and suppresses the precipitation over the WNP (Wang et  
335 al., 2015). It affects the Asian monsoon by the meridional asymmetry of the monsoonal  
336 easterly shear during the boreal summer, which can particularly strengthen the northern  
337 branch of the Rossby wave response to the south-eastern Indian Ocean SST cooling, leading  
338 to an intensified monsoon flow as well as an intensified convection (Wang and Xie,  
339 1996;Wang et al., 2003;Xiang et al., 2011;Wang et al., 2015). We noted that the models  
340 simulate a reasonable first EOF mode (Figure 3), but illustrate no skill in capturing the other  
341 EOF leading modes (not shown). We argue that the models cannot well represent the  
342 monsoon-ocean interaction, even with initialisation. Then, the models do not simulate the  
343 third EOF leading mode of the EASM since the predictability of the IOD extends only over a



344 three-month time-scale (Choudhury et al., 2015). The current initialisation strategies (both  
345 anomaly and full-field) enhance the ENSO signal in the model simulations with higher  
346 explained fraction of variance. Kim et al. (2012) described a similar finding in ECMWF  
347 System 4 and NCEP Climate Forecast System version 2 (CFSv2) seasonal prediction  
348 simulations. This overly strong modulation of the EASM by ENSO due to the models well  
349 predict ENSO on seasonal time-scale with initialisation (Kim et al., 2012; Jin et al., 2008).

350 It is worth mentioning that it was an extremely weak monsoon and strong El Niño  
351 year in 1998. The CanCM4, the GFDL-CM2p1, the MIROC5 and the MPI-ESM-LR have the  
352 ability to simulate the extreme monsoon event, while the BCC-CSM1-1, and the HadCM3 do  
353 not capture it even with initialisation. There is potential for the BCC-CSM and the HadCM  
354 models to improve the teleconnection between the ENSO and the EASM.

355 This study has discussed six CMIP5 models in predicting the EASM on seasonal  
356 time-scale. The six models are earth system coupled models which present a better SST-  
357 monsoon teleconnection than IRI (International Research Institute for Climate and Society)  
358 models (Barnston et al., 2010) and CMIP3 models (Sperber et al., 2013). The CMIP5 models  
359 show a comparable prediction skill as current seasonal forecast application systems, the  
360 ECMWF System and the NCEP CFS, respectively. Both the two application systems have  
361 low prediction skill of EASM (Jiang et al., 2013; Kim et al., 2012).

362 We have compared six CMIP5 systems with their respective initialisation strategies.  
363 The GFDL-CM2p1 and the MIROC5 have the potential to serve as seasonal forecast  
364 application system even with their current initialisation method. These models have great  
365 potential to optimise the SST-EASM interaction simulation performance to improve their  
366 seasonal prediction skill of the EASM.

### 367 **Acknowledgements**

368 This work was supported by the China Scholarship Council (CSC) and the Freie Universität  
369 Berlin. We would like to thank the climate modelling groups listed in Table 1 of this paper  
370 for producing and making their model output available. We acknowledge the MiKlip project  
371 funded by the Federal Ministry of Education and Research and the German Climate  
372 Computing Centre (DKRZ) for providing the data services.

### 373 **References**

374 Adler, R. F., Huffman, G. J., Chang, A., Ferraro, R., Xie, P.-P., Janowiak, J., Rudolf, B.,  
375 Schneider, U., Curtis, S., Bolvin, D., Gruber, A., Susskind, J., Arkin, P., and Nelkin, E.: The  
376 Version-2 Global Precipitation Climatology Project (GPCP) Monthly Precipitation Analysis



- 377 (1979–Present), *J Hydrometeorol*, 4, 1147-1167, 10.1175/1525-  
378 7541(2003)004<1147:tvgpcc>2.0.co;2, 2003.
- 379 Arora, V. K., Scinocca, J. F., Boer, G. J., Christian, J. R., Denman, K. L., Flato, G. M.,  
380 Kharin, V. V., Lee, W. G., and Merryfield, W. J.: Carbon emission limits required to satisfy  
381 future representative concentration pathways of greenhouse gases, *Geophys Res Lett*, 38,  
382 L05805, 10.1029/2010gl046270, 2011.
- 383 Barnett, T. P., and Schlesinger, M. E.: Detecting Changes in Global Climate Induced by  
384 Greenhouse Gases, *J Geophys Res Atmos*, 92, 14772-14780, 10.1029/JD092iD12p14772,  
385 1987.
- 386 Barnston, A. G., Li, S. H., Mason, S. J., DeWitt, D. G., Goddard, L., and Gong, X. F.:  
387 Verification of the First 11 Years of IRI's Seasonal Climate Forecasts, *J Appl Meteorol Clim*,  
388 49, 493-520, 10.1175/2009jamc2325.1, 2010.
- 389 Choi, J., Son, S. W., Ham, Y. G., Lee, J. Y., and Kim, H. M.: Seasonal-to-Interannual  
390 Prediction Skills of Near-Surface Air Temperature in the CMIP5 Decadal Hindcast  
391 Experiments, *J Clim*, 29, 1511-1527, 10.1175/Jcli-D-15-0182.1, 2016.
- 392 Choudhury, D., Sharma, A., Sivakumar, B., Sen Gupta, A., and Mehrotra, R.: On the  
393 predictability of SSTA indices from CMIP5 decadal experiments, *Environ Res Lett*, 10,  
394 074013, 10.1088/1748-9326/10/7/074013, 2015.
- 395 Dee, D. P., Uppala, S. M., Simmons, A. J., Berrisford, P., Poli, P., Kobayashi, S., Andrae, U.,  
396 Balmaseda, M. A., Balsamo, G., Bauer, P., Bechtold, P., Beljaars, A. C. M., van de Berg, L.,  
397 Bidlot, J., Bormann, N., Delsol, C., Dragani, R., Fuentes, M., Geer, A. J., Haimberger, L.,  
398 Healy, S. B., Hersbach, H., Holm, E. V., Isaksen, I., Kallberg, P., Kohler, M., Matricardi, M.,  
399 McNally, A. P., Monge-Sanz, B. M., Morcrette, J. J., Park, B. K., Peubey, C., de Rosnay, P.,  
400 Tavolato, C., Thepaut, J. N., and Vitart, F.: The ERA-Interim reanalysis: configuration and  
401 performance of the data assimilation system, *Q J R Meteorolog Soc*, 137, 553-597,  
402 10.1002/qj.828, 2011.
- 403 Delworth, T. L., Broccoli, A. J., Rosati, A., Stouffer, R. J., Balaji, V., Beesley, J. A., Cooke,  
404 W. F., Dixon, K. W., Dunne, J., Dunne, K. A., Durachta, J. W., Findell, K. L., Ginoux, P.,  
405 Gnanadesikan, A., Gordon, C. T., Griffies, S. M., Gudgel, R., Harrison, M. J., Held, I. M.,  
406 Hemler, R. S., Horowitz, L. W., Klein, S. A., Knutson, T. R., Kushner, P. J., Langenhorst, A.  
407 R., Lee, H. C., Lin, S. J., Lu, J., Malyshev, S. L., Milly, P. C. D., Ramaswamy, V., Russell, J.,  
408 Schwarzkopf, M. D., Shevliakova, E., Sirutis, J. J., Spelman, M. J., Stern, W. F., Winton, M.,  
409 Wittenberg, A. T., Wyman, B., Zeng, F., and Zhang, R.: GFDL's CM2 global coupled climate  
410 models. Part I: Formulation and simulation characteristics, *J Clim*, 19, 643-674,  
411 10.1175/Jcli3629.1, 2006.
- 412 Ding, Y.: Seasonal march of the East-Asian summer monsoon., in: *East Asian Monsoon*,  
413 edited by: Chang, C.-P., World Scientific, Singapore, 560, 2004.
- 414 Ding, Y. H.: *Monsoons over China*, Kluwer Academic Publisher, Dordrecht/Boston/London,  
415 419 pp., 1994.
- 416 Ding, Y. H., and Chan, J. C. L.: The East Asian summer monsoon: an overview, *Meteorol*  
417 *Atmos Phys*, 89, 117-142, 10.1007/s00703-005-0125-z, 2005.
- 418 Drosowsky, W., and Zhang, H.: Verification of Spatial Fields, in: *Forecast Verification: A*  
419 *Practitioner's Guide in Atmospheric Science* edited by: Jolliffe, L. T., and Stephenson, D. B.,  
420 John Wiley & Sons Ltd, England, 128-129, 2003.
- 421 Huang, B. Y., Banzon, V. F., Freeman, E., Lawrimore, J., Liu, W., Peterson, T. C., Smith, T.  
422 M., Thorne, P. W., Woodruff, S. D., and Zhang, H. M.: Extended Reconstructed Sea Surface  
423 Temperature Version 4 (ERSST.v4). Part I: Upgrades and Intercomparisons, *J Clim*, 28, 911-  
424 930, 10.1175/Jcli-D-14-00006.1, 2015.



- 425 Jiang, X. W., Yang, S., Li, Y. Q., Kumar, A., Liu, X. W., Zuo, Z. Y., and Jha, B.: Seasonal-  
426 to-Interannual Prediction of the Asian Summer Monsoon in the NCEP Climate Forecast  
427 System Version 2, *J Clim*, 26, 3708-3727, 10.1175/Jcli-D-12-00437.1, 2013.
- 428 Jin, E. K., Kinter, J. L., Wang, B., Park, C. K., Kang, I. S., Kirtman, B. P., Kug, J. S., Kumar,  
429 A., Luo, J. J., Schemm, J., Shukla, J., and Yamagata, T.: Current status of ENSO prediction  
430 skill in coupled ocean-atmosphere models, *Clim Dyn*, 31, 647-664, 10.1007/s00382-008-  
431 0397-3, 2008.
- 432 Kang, I.-S., and Shukla, J.: Dynamic seasonal prediction and predictability of the monsoon,  
433 in: *The Asian Monsoon*, edited by: Wang, B., Springer Berlin Heidelberg, Berlin, Heidelberg,  
434 585-612, 2006.
- 435 Kang, I. S., Lee, J. Y., and Park, C. K.: Potential predictability of summer mean precipitation  
436 in a dynamical seasonal prediction system with systematic error correction, *J Clim*, 17, 834-  
437 844, 10.1175/1520-0442(2004)017<0834:Pposmp>2.0.Co;2, 2004.
- 438 Kang, I. S., and Yoo, J. H.: Examination of multi-model ensemble seasonal prediction  
439 methods using a simple climate system, *Clim Dyn*, 26, 285-294, 10.1007/s00382-005-0074-8,  
440 2006.
- 441 Kim, H. J., Wang, B., and Ding, Q. H.: The Global Monsoon Variability Simulated by  
442 CMIP3 Coupled Climate Models, *J Clim*, 21, 5271-5294, 10.1175/2008jcli2041.1, 2008.
- 443 Kim, H. J., Takata, K., Wang, B., Watanabe, M., Kimoto, M., Yokohata, T., and Yasunari, T.:  
444 Global Monsoon, El Nino, and Their Interannual Linkage Simulated by MIROC5 and the  
445 CMIP3 CGCMs, *J Clim*, 24, 5604-5618, 10.1175/2011jcli4132.1, 2011.
- 446 Kim, H. M., Webster, P. J., Curry, J. A., and Toma, V. E.: Asian summer monsoon prediction  
447 in ECMWF System 4 and NCEP CFSv2 retrospective seasonal forecasts, *Clim Dyn*, 39,  
448 2975-2991, 10.1007/s00382-012-1470-5, 2012.
- 449 Lee, J.-Y., Wang, B., Kang, I. S., Shukla, J., Kumar, A., Kug, J. S., Schemm, J. K. E., Luo, J.  
450 J., Yamagata, T., Fu, X., Alves, O., Stern, B., Rosati, T., and Park, C. K.: How are seasonal  
451 prediction skills related to models' performance on mean state and annual cycle?, *Clim Dyn*,  
452 35, 267-283, 10.1007/s00382-010-0857-4, 2010.
- 453 Luo, J.-J., Masson, S., Behera, S. K., and Yamagata, T.: Extended ENSO Predictions Using a  
454 Fully Coupled Ocean-Atmosphere Model, *J Clim*, 21, 84-93, 10.1175/2007jcli1412.1, 2008.
- 455 Magnusson, L., Alonso-Balmaseda, M., Corti, S., Molteni, F., and Stockdale, T.: Evaluation  
456 of forecast strategies for seasonal and decadal forecasts in presence of systematic model  
457 errors, *Clim Dyn*, 41, 2393-2409, 10.1007/s00382-012-1599-2, 2013.
- 458 Matei, D., Pohlmann, H., Jungclaus, J., Muller, W., Haak, H., and Marotzke, J.: Two Tales of  
459 Initializing Decadal Climate Prediction Experiments with the ECHAM5/MPI-OM Model, *J*  
460 *Clim*, 25, 8502-8523, 10.1175/Jcli-D-11-00633.1, 2012.
- 461 Meehl, G., Covey, C., Delworth, T., Latif, M., McAvaney, B., Mitchell, J., Stouffer, R., and  
462 Taylor, K.: The WCRP CMIP3 multi-model dataset: a new era in climate change research,  
463 *Bull Am Meteorol Soc*, 88, 1383-1394, 2007.
- 464 Meehl, G. A., Goddard, L., Murphy, J., Stouffer, R. J., Boer, G., Danabasoglu, G., Dixon, K.,  
465 Giorgetta, M. A., Greene, A. M., Hawkins, E., Hegerl, G., Karoly, D., Keenlyside, N.,  
466 Kimoto, M., Kirtman, B., Navarra, A., Pulwarty, R., Smith, D., Stammer, D., and Stockdale,  
467 T.: DECADAL PREDICTION Can It Be Skillful?, *Bull Am Meteorol Soc*, 90, 1467-1485,  
468 10.1175/2009bams2778.1, 2009.
- 469 Meehl, G. A., and Teng, H. Y.: Case studies for initialized decadal hindcasts and predictions  
470 for the Pacific region, *Geophys Res Lett*, 39, L22705, 10.1029/2012gl053423, 2012.
- 471 Meehl, G. A., Goddard, L., Boer, G., Burgman, R., Branstator, G., Cassou, C., Corti, S.,  
472 Danabasoglu, G., Doblas-Reyes, F., Hawkins, E., Karspeck, A., Kimoto, M., Kumar, A.,  
473 Matei, D., Mignot, J., Msadek, R., Navarra, A., Pohlmann, H., Rienecker, M., Rosati, T.,  
474 Schneider, E., Smith, D., Sutton, R., Teng, H. Y., van Oldenborgh, G. J., Vecchi, G., and



- 475 Yeager, S.: DECADAL CLIMATE PREDICTION An Update from the Trenches, *Bull Am*  
476 *Meteorol Soc*, 95, 243-267, 10.1175/Bams-D-12-00241.1, 2014.
- 477 Mitchell, J. F. B., Karoly, D. J., Hegerl, G. C., Zwiers, F. W., Allen, M. R., and Marengo, J.:  
478 Detection of Climate Change and Attribution of Causes, in: *Third Assessment Report of the*  
479 *Intergovernmental Panel on Climate Change.*, edited by: Houghton, J. T., Griggs, D. J.,  
480 Noguer, M., van der Linden, P. J., Dai, X., Maskell, K., and Johnson, C. A., Cambridge  
481 University Press, New York, 470, 2001.
- 482 Seo, K. H., Son, J. H., Lee, J. Y., and Park, H. S.: Northern East Asian Monsoon Precipitation  
483 Revealed by Airmass Variability and Its Prediction, *J Clim*, 28, 6221-6233, 10.1175/Jcli-D-  
484 14-00526.1, 2015.
- 485 Smith, D. M., Eade, R., and Pohlmann, H.: A comparison of full-field and anomaly  
486 initialization for seasonal to decadal climate prediction, *Clim Dyn*, 41, 3325-3338,  
487 10.1007/s00382-013-1683-2, 2013.
- 488 Sperber, K., Annamalai, H., Kang, I. S., Kitoh, A., Moise, A., Turner, A., Wang, B., and  
489 Zhou, T.: The Asian summer monsoon: an intercomparison of CMIP5 vs. CMIP3 simulations  
490 of the late 20th century, *Clim Dyn*, 41, 2711-2744, 10.1007/s00382-012-1607-6, 2013.
- 491 Sperber, K. R., Brankovic, C., Deque, M., Frederiksen, C. S., Graham, R., Kitoh, A.,  
492 Kobayashi, C., Palmer, T., Puri, K., Tennant, W., and Volodin, E.: Dynamical seasonal  
493 predictability of the Asian summer monsoon, *Mon Weather Rev*, 129, 2226-2248,  
494 10.1175/1520-0493(2001)129<2226:Dspota>2.0.Co;2, 2001.
- 495 Tao, S. Y., and Chen, L. X.: A review of recent research on the East Asian summer monsoon  
496 in China, in: *Monsoon Meteorology*, edited by: Chang, C.-P., and Krishnamurti, T. N., Oxford  
497 University Press, Oxford, 60-92, 1987.
- 498 Tatebe, H., Ishii, M., Mochizuki, T., Chikamoto, Y., Sakamoto, T. T., Komuro, Y., Mori, M.,  
499 Yasunaka, S., Watanabe, M., Ogochi, K., Suzuki, T., Nishimura, T., and Kimoto, M.: The  
500 Initialization of the MIROC Climate Models with Hydrographic Data Assimilation for  
501 Decadal Prediction, *J Meteorol Soc Japan*, 90a, 275-294, 10.2151/jmsj.2012-A14, 2012.
- 502 Taylor, K. E., Stouffer, R. J., and Meehl, G. A.: An Overview of Cmp5 and the Experiment  
503 Design, *Bull Am Meteorol Soc*, 93, 485-498, 10.1175/Bams-D-11-00094.1, 2012.
- 504 Wang, B., and Xie, X.: Low-Frequency Equatorial Waves in Vertically Sheared Zonal Flow.  
505 Part I: Stable Waves, *J Atmos Sci*, 53, 449-467, 10.1175/1520-  
506 0469(1996)053<0449:lfewiv>2.0.co;2, 1996.
- 507 Wang, B., and Fan, Z.: Choice of south Asian summer monsoon indices, *Bull Am Meteorol*  
508 *Soc*, 80, 629-638, 10.1175/1520-0477(1999)080<0629:Cosasm>2.0.Co;2, 1999.
- 509 Wang, B., Wu, R. G., and Fu, X. H.: Pacific-East Asian teleconnection: how does ENSO  
510 affect East Asian climate?, *J Clim*, 13, 1517-1536, 2000.
- 511 Wang, B., Wu, R., and Li, T.: Atmosphere–Warm Ocean Interaction and Its Impacts on  
512 Asian–Australian Monsoon Variation\*, *J Clim*, 16, 1195-1211, 10.1175/1520-  
513 0442(2003)16<1195:aoiaii>2.0.co;2, 2003.
- 514 Wang, B., Kang, I.-S., and Lee, J.-Y.: Ensemble Simulations of Asian–Australian Monsoon  
515 Variability by 11 AGCMs\*, *J Clim*, 17, 803-818, 10.1175/1520-  
516 0442(2004)017<0803:esoamv>2.0.co;2, 2004.
- 517 Wang, B., Ding, Q. H., Fu, X. H., Kang, I. S., Jin, K., Shukla, J., and Doblas-Reyes, F.:  
518 Fundamental challenge in simulation and prediction of summer monsoon rainfall, *Geophys*  
519 *Res Lett*, 32, L15711, 10.1029/2005gl022734, 2005.
- 520 Wang, B.: *The Asian Monsoon*, Springer Science & Business Media, Praxis, New York, NY,  
521 USA, 2006.
- 522 Wang, B., Lee, J.-Y., Kang, I. S., Shukla, J., Kug, J. S., Kumar, A., Schemm, J., Luo, J. J.,  
523 Yamagata, T., and Park, C. K.: How accurately do coupled climate models predict the leading



- 524 modes of Asian-Australian monsoon interannual variability?, *Clim Dyn*, 30, 605-619,  
525 10.1007/s00382-007-0310-5, 2007.
- 526 Wang, B., Lee, J.-Y., Kang, I.-S., Shukla, J., Park, C. K., Kumar, A., Schemm, J., Cocke, S.,  
527 Kug, J. S., Luo, J. J., Zhou, T., Wang, B., Fu, X., Yun, W. T., Alves, O., Jin, E. K., Kinter, J.,  
528 Kirtman, B., Krishnamurti, T., Lau, N. C., Lau, W., Liu, P., Pegion, P., Rosati, T., Schubert,  
529 S., Stern, W., Suarez, M., and Yamagata, T.: Advance and prospectus of seasonal prediction:  
530 assessment of the APCC/CliPAS 14-model ensemble retrospective seasonal prediction  
531 (1980–2004), *Clim Dyn*, 33, 93-117, 10.1007/s00382-008-0460-0, 2008a.
- 532 Wang, B., Wu, Z. W., Li, J. P., Liu, J., Chang, C. P., Ding, Y. H., and Wu, G. X.: How to  
533 measure the strength of the East Asian summer monsoon, *J Clim*, 21, 4449-4463,  
534 10.1175/2008jcli2183.1, 2008b.
- 535 Wang, B., Xiang, B., and Lee, J. Y.: Subtropical high predictability establishes a promising  
536 way for monsoon and tropical storm predictions, *Proc Natl Acad Sci U S A*, 110, 2718-2722,  
537 10.1073/pnas.1214626110, 2013.
- 538 Wang, B., Lee, J. Y., and Xiang, B. Q.: Asian summer monsoon rainfall predictability: a  
539 predictable mode analysis, *Clim Dyn*, 44, 61-74, 10.1007/s00382-014-2218-1, 2015.
- 540 Wu, R. G., Hu, Z. Z., and Kirtman, B. P.: Evolution of ENSO-related rainfall anomalies in  
541 East Asia, *J Clim*, 16, 3742-3758, 10.1175/1520-0442(2003)016<3742:Eoerai>2.0.Co;2,  
542 2003.
- 543 Wu, T. W., Song, L. C., Li, W. P., Wang, Z. Z., Zhang, H., Xin, X. G., Zhang, Y. W., Zhang,  
544 L., Li, J. L., Wu, F. H., Liu, Y. M., Zhang, F., Shi, X. L., Chu, M., Zhang, J., Fang, Y. J.,  
545 Wang, F., Lu, Y. X., Liu, X. W., Wei, M., Liu, Q. X., Zhou, W. Y., Dong, M., Zhao, Q. G., Ji,  
546 J. J., Li, L., and Zhou, M. Y.: An Overview of BCC Climate System Model Development and  
547 Application for Climate Change Studies, *J Meteorol Res-Prc*, 28, 34-56, 10.1007/s13351-  
548 014-3041-7, 2014.
- 549 Wu, Z. W., Wang, B., Li, J. P., and Jin, F. F.: An empirical seasonal prediction model of the  
550 east Asian summer monsoon using ENSO and NAO, *J Geophys Res Atmos*, 114, D18120,  
551 10.1029/2009jd011733, 2009.
- 552 Xiang, B., Wang, B., Yu, W., and Xu, S.: How can anomalous western North Pacific  
553 Subtropical High intensify in late summer?, *Geophys Res Lett*, 40, 2349-2354,  
554 10.1002/grl.50431, 2013.
- 555 Xiang, B. Q., Yu, W. D., Li, T., and Wang, B.: The critical role of the boreal summer mean  
556 state in the development of the IOD, *Geophys Res Lett*, 38, L02710, 10.1029/2010gl045851,  
557 2011.
- 558 Yang, S., Zhang, Z. Q., Kousky, V. E., Higgins, R. W., Yoo, S. H., Liang, J. Y., and Fan, Y.:  
559 Simulations and seasonal prediction of the Asian summer monsoon in the NCEP Climate  
560 Forecast System, *J Clim*, 21, 3755-3775, 10.1175/2008jcli1961.1, 2008.
- 561 Yim, S. Y., Wang, B., and Xing, W.: Prediction of early summer rainfall over South China by  
562 a physical-empirical model, *Clim Dyn*, 43, 1883-1891, 10.1007/s00382-013-2014-3, 2014.
- 563 Zhou, T., Wu, B., and Wang, B.: How Well Do Atmospheric General Circulation Models  
564 Capture the Leading Modes of the Interannual Variability of the Asian–Australian Monsoon?,  
565 *J Clim*, 22, 1159-1173, 10.1175/2008jcli2245.1, 2009.
- 566 Zhou, T. J., and Yu, R. C.: Atmospheric water vapor transport associated with typical  
567 anomalous summer rainfall patterns in China, *J Geophys Res Atmos*, 110, D08104,  
568 10.1029/2004jd005413, 2005.

569



Table 1. Details of the prediction systems investigated in this study.

System	Institute	Resolution		Initialisation		Reference	
		Atmospheric	Oceanic	Members	Type		
<b>BCC-</b>	Beijing Climate Center,	T42L26	1lonx1.33lat	3	3	Full-field	Wu <i>et al.</i> (2014)
<b>CSMI-1</b>	China		L40				
<b>CanCM4</b>	Canadian Centre for Climate Modelling and Analysis,	T63L35	256 x 192	10	10	Full-field	Arora <i>et al.</i> (2011)
	Canada		L40				
<b>GFDL-</b>	Geophysical Fluid	N45L24	1lon x 0.33-	10	10	Full-field	Delworth <i>et al.</i> (2006)
<b>CM2p1</b>	Dynamics Laboratory, USA		1lat L50				
<b>HadCM3</b>	Met Office Hadley Centre, UK	N48L19	1.25x1.25	10	10 + 10	Full-field and Anomaly	Smith <i>et al.</i> (2013)
			L20				
<b>MIROC5</b>	Atmosphere and Ocean Research Institute, Japan	T85L40	256x192 L44	5	6	Anomaly	Tatebe <i>et al.</i> (2012)
<b>MPI-ESM-</b>	Max Planck Institute for	T63L47	GR15 L40	3	3	Anomaly	Matei <i>et al.</i> (2012)
<b>LR</b>	Meteorology, Germany						



572 Table 2. Brief summaries of initialisation strategies used by modelling groups in the study. ECMWF: European Centre for Medium-Range  
 573 Weather Forecasts; GODAS: Global Ocean Data Assimilation System; NCEP: National Centers for Environmental Prediction; S: Salinity;  
 574 SODA: Simple Ocean Data Assimilation; T: Temperature.

system	Atmosphere	Ocean	Internet
<b>BCC-CSM1-1</b>	-	integration with ocean T nudged to SODA product above 1500 m	<a href="http://forecast.bccesm.ncc-cma.net/">http://forecast.bccesm.ncc-cma.net/</a>
<b>CanCM4</b>	ECMWF re-analysis	off-line assimilation of SODA and GODAS subsurface ocean T and S adjusted to reserve model T-S	<a href="http://www.cccma.ec.gc.ca/">http://www.cccma.ec.gc.ca/</a>
<b>GFDL-CM2p1</b>	GFDL re-analysis	assimilates observations of T, S from World Ocean Database	<a href="https://www.gfdl.noaa.gov/multidecadal-prediction-stream/">https://www.gfdl.noaa.gov/multidecadal-prediction-stream/</a>
<b>HadCM3</b>	ECMWF re-analysis	off-line ocean re-analysis product	<a href="http://cerawww.dkrz.de/WDCC/CMIP5/">http://cerawww.dkrz.de/WDCC/CMIP5/</a>
<b>MIROC5</b>	-	integration using observational gridded ocean T and S	<a href="http://amaterasu.ees.hokudai.ac.jp/">http://amaterasu.ees.hokudai.ac.jp/</a>
<b>MPI-ESM-LR</b>	NCEP re-analysis	off-line ocean hindcast forced with NCEP	<a href="http://cerawww.dkrz.de/WDCC/CMIP5/">http://cerawww.dkrz.de/WDCC/CMIP5/</a>

575  
 576  
 577

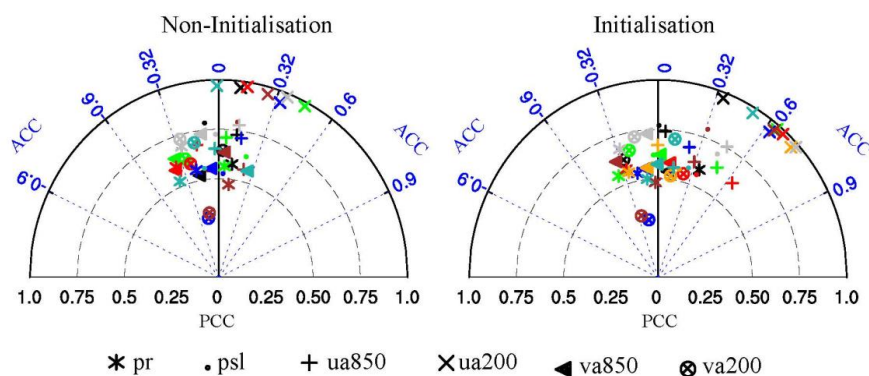


578  
 579 Table 3. Description of the six variables which contribute to the EASM. The abbreviation of these variables is followed to the guidelines of  
 580 CMIP5.

variable	Standard name	Contribution to the EASM
pr	Precipitation	Precipitation distribution indicates the strength of EASM
psl	Mean sea surface pressure	Differences of mean sea surface pressure between land and ocean lead to EASM
ua850	Zonal winds over 850 hPa	A component of low-level cyclone which transports vapor from ocean to land
va850	Meridional winds over 850 hPa	As ua850, and contributes to Hadley's cell
ua200	Zonal winds over 850 hPa	A component of upper-level Hadley's cell
va200	Meridional winds over 850 hPa	As ua200



581



582

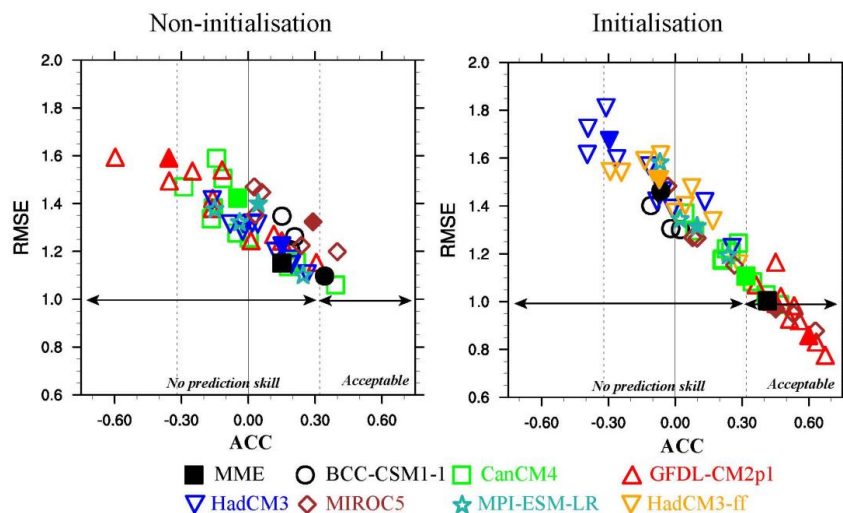
583 Fig. 1. Taylor diagrams display of pattern (PCC) and temporal (ACC) correlation  
 584 metrics of six variables between observation and model simulation in the EASM  
 585 region (0-50°N, 100-140°E). Each coloured marker represents a model, *i.e.*, the BCC-  
 586 CSM1-1 (black), the CanCM4 (green), the GFDL-CM2p1 (red), the HadCM3 (blue),  
 587 the MIROC5 (brown), the MPI-ESM-LR (light-sea-blue), and the HadCM3-ff  
 588 (*i.e.*, psl) were compared by ERA-Interim re-analysis.  
 589 while wind fields (*i.e.*, ua850, va850, ua200 and va200) and mean sea level pressure  
 590 (*i.e.*, psl) were compared by ERA-Interim re-analysis.

591



592

593



594

595 Fig. 2. Performance of the model ensemble member (hollow marker) and its ensemble  
 596 mean (solid marker) on the EASM index. The abscissa and ordinates are the anomaly  
 597 correlation coefficient (ACC) and the root-mean-square-error (RMSE), respectively.

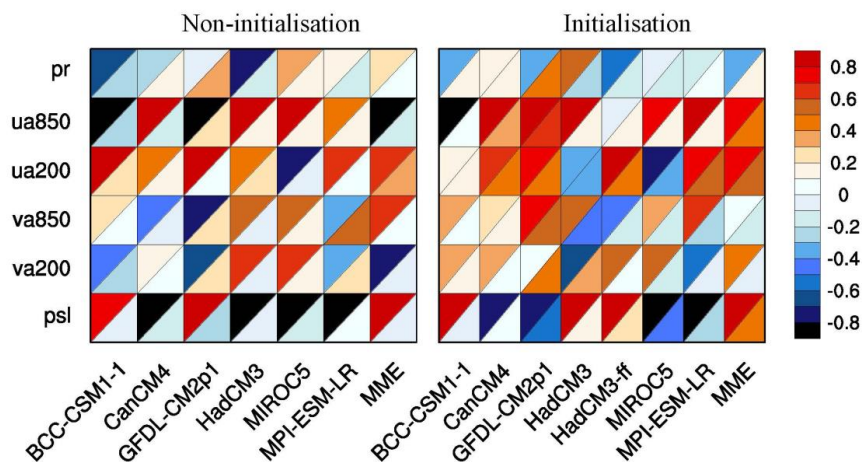
598 The observed EASM index is calculated by zonal wind at 850 hPa from the ERA-  
 599 Interim re-analysis data. The black dot lines indicate the significant level at 0.1. The  
 600 vertical black line represents the correlation between the simulating and the  
 601 observational EASM index is 0.

602



603

604



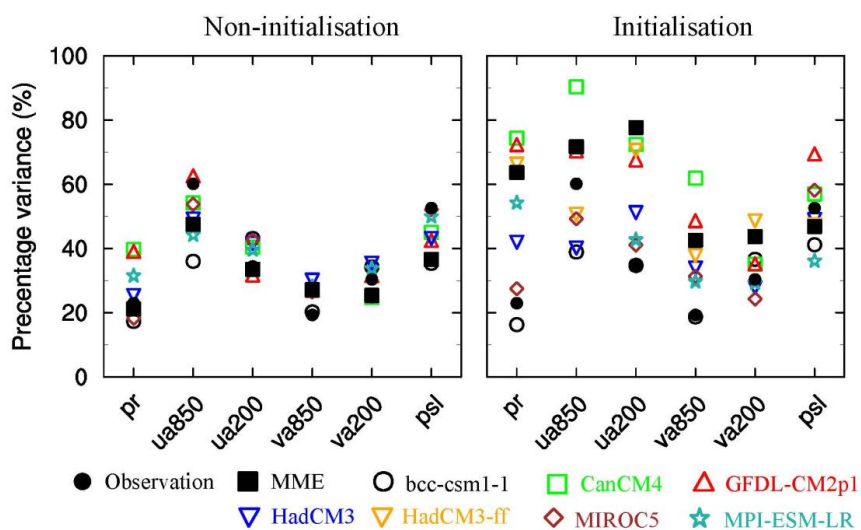
605

606 Fig. 3. Portrait diagram display of correlation metrics between the observation and the  
607 model simulation of the first lead EOF mode for the six fields in the non-initialisation  
608 (left) and the initialisation (right). Each grid square is split by a diagonal in order to  
609 show the correlation with respect to both the eigenvector (upper left triangle) and its  
610 associated principal components (lower right triangle) reference data sets.

611



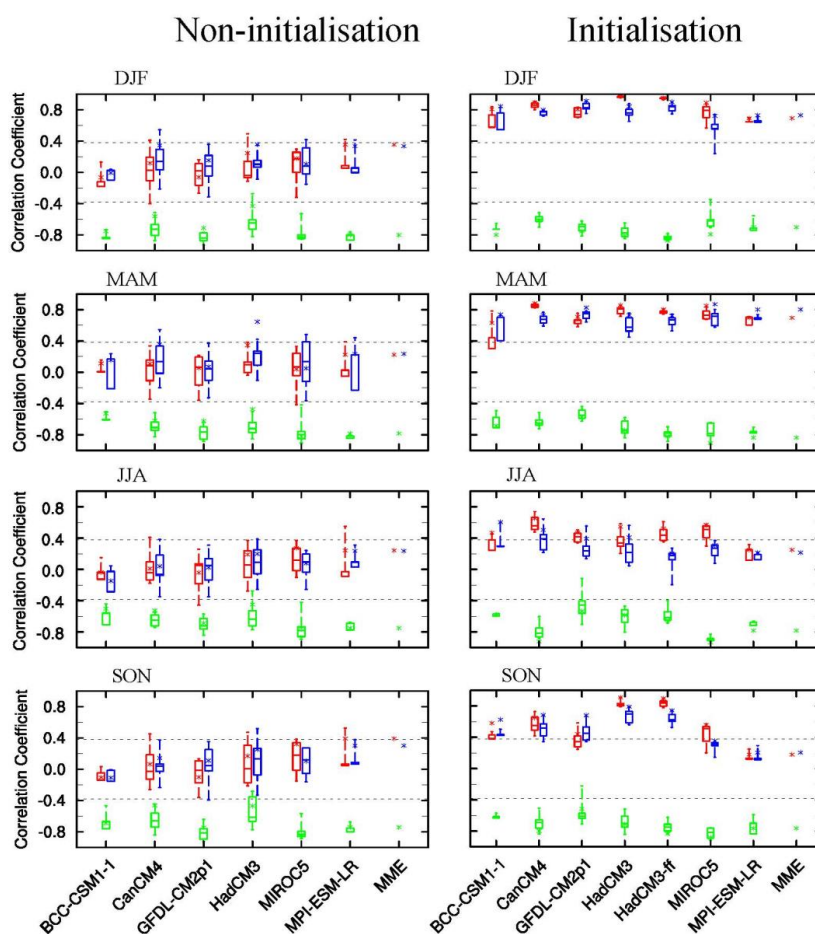
612



613

614 Fig. 4. Fraction variance (%) explained by the first EOF mode for six fields in the  
 615 non-initialisation (left) and the initialisation (right).

616



617

618 Fig. 5. Model prediction skill in representing the observational Niño3.4 (red), the SOI  
 619 (blue) from the DJF to SON in non-initialisation (left) and initialisation (right). Green  
 620 diagram shows the correlation coefficient between the model simulated Niño3.4 and  
 621 the SOI. Box and whisker diagram shows ensemble mean of each model (asterisk),  
 622 median (horizontal line), 25th and 75th percentiles (box), minimum and maximum  
 623 (whisker). The two black dotted lines indicate 0.05 significant level based upon  
 624 Student's t-test.

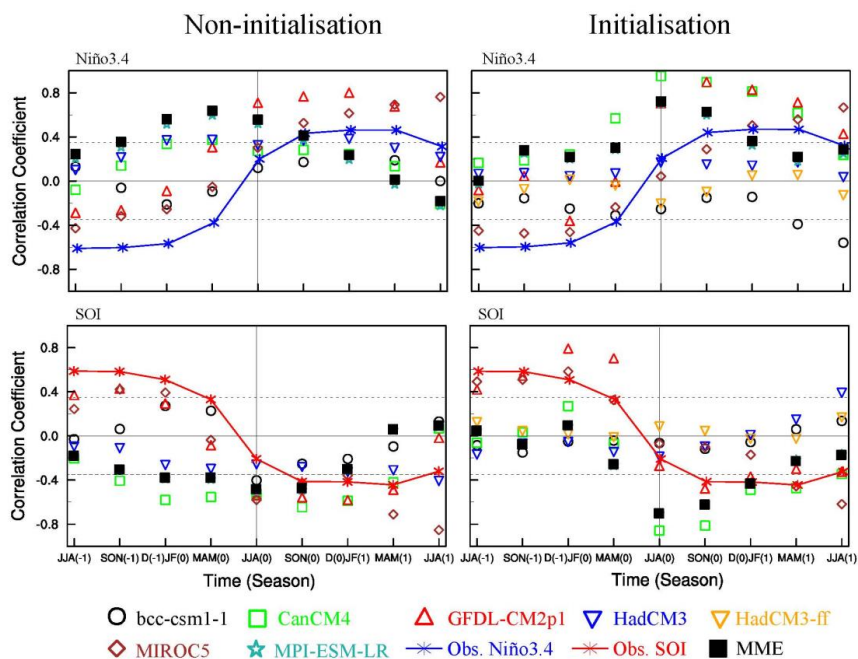
625

626

627



628



629

630 Fig. 6. Lead-lag correlation coefficients between the EASM index and Niño3.4  
 631 (upper), and SOI (lower) in non-initialised simulations (left) and initialised ones  
 632 (right) for observation (marker line) and models (marker) from JJA(-1) to JJA(+1).  
 633 The two black dotted lines are 0.05 significant level based upon Student's t-test. The  
 634 vertical line represents JJA(0), where the simultaneous correlations between the  
 635 EASM index and Niño3.4, and SOI are shown.

636